Supplementary Materials for

Personalized predictions and non-invasive imaging of human brain temperature

Dongsuk Sung, Peter A. Kottke, Benjamin B. Risk, Jason W. Allen, Fadi Nahab, Andrei G. Fedorov,* and Candace C. Fleischer*

*Corresponding author emails: candace.fleischer@emory.edu (C.C.F.); andrei.fedorov@me.gatech.edu (A.G.F.)

This file includes:

Supplementary Methods: Model Details, Derivation, and Numerical Solution

1. Blood Vessel Flow: Mass Conservation and Vessel Geometry

Blood vessels (arteries and veins) are modeled as 1D networks of line segments connected at nodes, all embedded within a 3D discretized brain domain which consists of grey matter, white matter, cerebrospinal fluid, bone, and scalp. Blood vessel nodes (segment endpoints) are points where flow can split or combine. In our model, which is based on the VaPor model[1], the terminal segments of the blood vessel network are arterioles and venules at the point where they split into capillary beds. Blood flow in capillaries is treated as flow in an isotropic porous medium, i.e., the blood in the capillaries is assumed to be in local thermal equilibrium with the surrounding tissue. Therefore, blood flow to tissue from arteries (from domain 1 to 2), and from tissue to veins (from domain 2 to 3), is modelled as occurring only from terminal segments. The model is simplified by assuming this blood flow occurs at a uniform mass flow rate per unit length of blood vessel segment as described in the Methods section, *MR inputs and parameters for the model*. The mass flow rate within each blood vessel segment, $\dot{F}$, is then found such that mass conservation is maintained for each node *j*, i.e., $\sum_{\text{in}} \dot{F} - \sum_{\text{out}} \dot{F} = \pm \sum_{\text{terminal}} \dot{F}$, where the first summation is over all non-terminal inlet segments meeting at the node (segments coming from lower numbered nodes), the second summation is over all non-terminal outlet segments meeting at the node (segments leading to higher numbered nodes), and the third summation is over all terminal segments sharing the node, and its preceding operator is subtraction for veins and addition for arteries. A negative value for a given $\dot{F}$ in the first two summations indicates that the flow direction is from a higher to lower numbered node. The resulting sparse system of algebraic equations is closed through specification of the inlet and outlet flow rates. The overall mass flow rate of blood into and out of the brain, $\dot{F}_{\text{tot}}$, is specified and split into 3 inlets based on an assumed distribution of 40% into each of the left and right internal carotid arteries and 20% into the basilar artery, and evenly distributed (50% of the total flow rate through each) exiting the brain through each transverse sinus. Vessel diameters are determined *posteriori* at the nodes based on the empirical relationship $D = 0.0332\dot{F}^{0.3703}$. The diameter at terminal nodes (where mass flow rate is zero), is taken to be 10 μm (the diameter assumed for capillaries throughout the brain). This approach to vessel flow rate estimation and diameter does not link pressures in the vessels and the tissue (i.e., mass conservation is imposed but momentum conservation between the vessels and tissue is not) and relies on the fact that the vessel modeling process avoids vessel interconnections. Vessel geometry (surface area) and lengths are estimated assuming straight line segments with a circular cross section and linearly varying diameter between nodes.

2. Capillary Blood Flow (Blood Flow in Tissue): Mass Conservation and Pressure Distribution

Blood flow to tissue from arteries, and from tissue to veins, is modelled as occurring only from terminal segments and is assumed to occur at a uniform rate per unit length of blood vessel segment as described in the Methods section, MR inputs and parameters for the model, and above. Tissue is discretized as voxels, which are cubes with edge length l_{voxel}. Properties within each voxel are derived based on assumed properties for grey matter, white matter, cerebrospinal fluid, bone, and scalp using probability weighted images; specific heats, thermal conductivities, densities, volumetric metabolic heat generation rates, and blood volume fractions, ε_{b}, are all calculated using volume based averaging within each voxel[1]. For capillary blood flow, the vasculature conductance

in a voxel, *G*, is obtained as in the VaPor model[1] using the volume averaged blood volume fraction in the voxel, ε_{b}, an assumed capillary diameter, D_{cap}, of 10 μm and capillary tortuosity, τ, of 2.5 using equation $G = \rho_{\mathrm{b}}\varepsilon_{\mathrm{b}} l_{\mathrm{voxel}}\pi D_{\mathrm{cap}}^2/(32\mu_{\mathrm{b}}\tau)$, where μ_{b} is the viscosity of blood. The pressure field in the tissue is found using a modified form of the Carman-Kozeny equation for each voxel *i*, $\sum_i \bar{G}_{ij}\left(P_i - P_j\right) = \dot{M}_{1\to2} - \dot{M}_{2\to3}$ where the summation is over all neighboring voxels, the mass source and sink terms account for all blood flow into and out of the voxel from blood vessels, and $\bar{G}_{ij}$ is the average conductance of voxel *i* and neighboring voxel *j*. This equation can be derived by combining the standard form of the Carman-Kozeny equation written for each direction, with the continuity equation written to account for mass source/sinks. The resulting system of equations yields a unique solution of pressure differences $\Delta P_{ij} = P_i - P_j$. These pressure differences can then be used to find the normal component of the velocities at the voxel boundaries, U_{ijn}, used in **Equations 1** and **3** by solving the standard form of the Carman-Kozeny equation written for each voxel boundary, i.e., $U_{ijn} = \bar{G}_{ij}\Delta P_{ij}/(\rho_{\mathrm{b}} l_{\mathrm{voxel}}^2)$.

3. Energy Conservation for Blood Vessels (Equations 1 and 3)

Numerical approximations of **Equations 1** and **3** are solved for control volumes based around blood vessel node *i* to find the mean blood temperature at each node. The control volume boundaries through which flow occurs are taken to be located at the segment midpoint between the nodes defining the segment. In **Equation 1**, the first term in the equation, representing the conductive heat transfer along the blood vessels, is numerically approximated using the temperature difference between nodes *i* and *j* and length of the connecting segment, l_{ij}, i.e., $\int_{A_{\mathrm{c}}} -K_{\mathrm{b}}\frac{\partial T_1}{\partial n}dA \approx -K_{\mathrm{b}}A_{\mathrm{c}}(\bar{T}_{1,j} - \bar{T}_{1,i})/l_{ij}$. The second term, which captures the advective transport of energy, is approximated using an upwinding scheme: $\int_{A_{\mathrm{c}}} \rho_{\mathrm{b}}c_{\mathrm{b}}U_{jn}T_1\,dA \approx c_{\mathrm{b}}\dot{F}_i\bar{T}_{1\mathrm{UW}}$ where $\bar{T}_{1\mathrm{UW}}$ is the upwinded temperature, i.e., the temperature of the node in the direction from which the blood is flowing. The third term, for the convective heat transfer between the blood vessel and the tissue, is approximated for each half-segment in the control volume using $\int_{L_a} hp_a(\bar{T}_1 - \bar{T}_2)dl \approx hA\sum_i \emptyset_{a,i}\,(\bar{T}_1 - \bar{T}_{2,i})$, where the summation is over all voxels intersected by the half-segment, and the prefactors $\emptyset_{a,i}$ denote the fraction of the overall length of the half-segment in voxel *i*. For simplicity, in both the VaPor model and in our application the prefactors are taken to be 1/*N* where *N* is the number of voxels intersected by the half-segment. The mean blood temperature driving convective heat transfer, $\bar{T}_1$, is approximated as the average of the mean blood temperatures at the segment endpoint nodes. The heat transfer coefficient, h, is estimated using a Nusselt number (dimensionless convective heat transfer coefficient) of 4 (based on fully developed flow in a circular pipe): $hA = 4\pi K_{\mathrm{b}} l$ where l is calculated for a half-segment assuming the blood vessel has a linearly varying diameter over its entire length between its value at the endpoint nodes, D_i and D_j, such that it is given by $l = \frac{1}{2}\sqrt{\left(D_i - D_j\right)^2 + l_{ij}^2}$. The last term in the equation accounts for the advective loss of energy with blood flow from the arteries and is nonzero only for control volumes that include terminal blood vessel segments, for which the term can be approximated as $\int_{L_a} c_{\mathrm{b}}\dot{M}'_{1\to2}\bar{T}_1 dl \approx c_{\mathrm{b}}\dot{M}_{1\to2}\bar{T}_1/2$ where the 2 accounts for the fact that the control volume contains only half the terminal segment, and $\bar{T}_1$ is the average of the mean blood temperatures at the segment endpoint nodes. The derivation and numerical approximation of **Equation 3** follows directly from that of **Equation 1**, *mutatis mutandis.*

4. Energy Conservation for Tissue (Equation 2)

The temperature of tissue and blood in capillaries is obtained for each voxel based on a numerical approximation of **Equation 2** which is derived using a control volume energy balance in a voxel. The first integral in **Equation 2** accounts for fluxes of energy across the control volume boundary to neighboring voxels and consists of two terms, one for conduction and one for advection. The first (conduction) term is approximated using a first order finite difference approximation: $\int_{A_{\text{voxel}}} -K\frac{\partial T_2}{\partial n}\,dA \approx -l_{\text{voxel}}\sum_j \bar{K}_j(\Delta\bar{T}_2)_{ij}$ where the summation is over all neighboring voxels, $\bar{K}_j$ is the average of the voxel being analyzed and neighboring voxel *j*'s thermal conductivities (which are themselves calculated using volume based averaging to account for composition of each voxel), and $(\Delta\bar{T}_2)_{ij}$ is the difference between the mean tissue temperature of voxel *i* and that of the voxel under consideration. The second (advection) term is approximated using an upwinding approach, $\int_{A_{\text{voxel}}} \rho_{\text{b}} c_{\text{b}} U_{2n} T_2\,dA \approx \rho_{\text{b}} c_{\text{b}} l_{\text{voxel}}^2 \sum_j U_{ijn}\bar{T}_{2\text{UW}}$ where the summation is over all voxels adjacent to voxel *i*, the U_{ijn} are the normal velocity components from voxel *i* to voxel *j*, and $\bar{T}_{2\text{UW}}$ is the upwinded temperature, i.e., the temperature of the node in the direction from which the blood is flowing.

The second integral in **Equation 2** accounts for the heat generation by metabolism and is the product of the voxel volume and the average volumetric metabolic heat generation in the voxel. The two remaining summations in **Equation 2** account for energy transport to the voxel from blood vessels that intersect the voxel and from the voxel to blood vessels, with the first summation representing the interaction with arteries and the second with veins. Focusing on the artery related summation, the numerical approximation is $\sum_a \emptyset_{a,i}\int_{L_a}\left[hp_a(\bar{T}_1-\bar{T}_2)+c_{\text{b}}\dot{M}'_{1\to2}\bar{T}_1\right]dl \approx \sum_a \emptyset_{a,i}\left[hA(\bar{T}_{a1}-\bar{T}_{i2})+c_{\text{b}}\dot{M}_{a1\to2}\bar{T}_{a1}\right]$ where the summation is over all arterial segments but the prefactor $\emptyset_{a,i}$ is nonzero only if the segment intersects voxel *i*: in that case it is 1/*N* where *N* is the total number of voxels intersected by arterial segment *a*. The first term in the brackets accounts for energy transport by convection from the blood in the arteries to the surrounding tissue, with the resistance being calculated as above in *3. Energy Conservation for Blood Vessels* (**Equations 1** and **3**) except the full segment length is used, i.e., the factor ½ does not appear in the definition of l. The mean blood temperature driving convective heat transfer (and also bringing in energy by advection), $\bar{T}_{a1}$, is approximated as the average of the mean blood temperatures at the segment endpoint nodes of arterial segment *a*, and $\bar{T}_{i2}$ is the tissue temperature in voxel *i*. $\dot{M}_{a1\to2}$ is the total mass flow rate from the segment so it is nonzero only for terminal segments.

5. Numerical Solution

The equations found by numerical approximation of **Equations 1**-**3** combined with boundary and inlet conditions form a system of linear algebraic equations for the unknown values of voxel and blood vessel node temperatures, which are compiled into a coefficient matrix, **A**, and a known vector, **b**; the vector whose unknown elements are sought after temperatures,**T**, is found using the matrix left division operator in MATLAB, i.e., $\mathbf{T} = \mathbf{A}\backslash\mathbf{b}$.

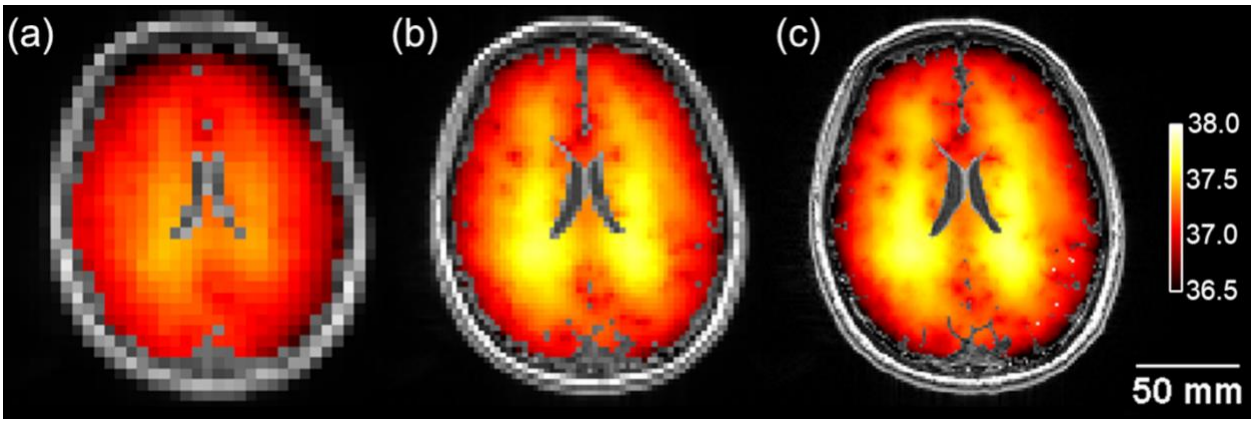

Supplementary Figure 1. Comparison of brain temperature maps generated with varied tissue voxel resolution. Model-predicted brain temperature maps from left to right for one subject using (a) coarsened ($5.2 \times 5.2 \times 4.0$ mm^3), (b) baseline ($2.6 \times 2.6 \times 2.0$ mm^3), and (c) refined ($1.3 \times 1.3 \times 1.0$ mm^3) voxel sizes. The coarsened model shows minimal spatial variation of temperature. The baseline temperature map had a tissue voxel resolution similar to the length of vessel segments from magnetic resonance (MR) angiography and venography (3 mm). Further refinement shows little difference in temperature distribution from that of the baseline voxel resolution, suggesting a voxel resolution less than or equal to the terminal vessel segment length is adequate to generate reproducible temperature maps with sufficient accuracy. Temperature color bar ranges from 36.5 to 38.0 ˚C. Scale bar is 50 mm and all images are on the same scale.

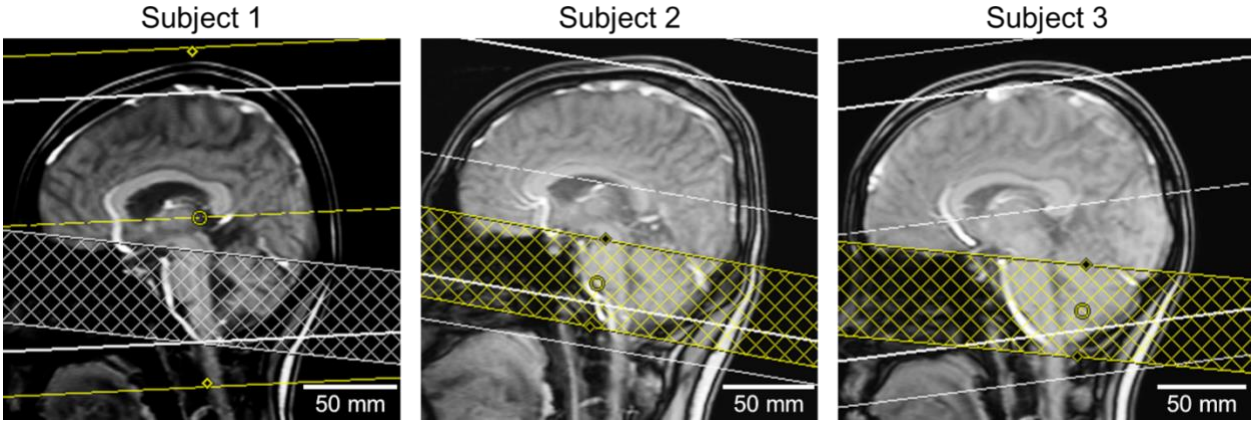

Supplementary Figure 2. Screenshots of the echo planar spectroscopic imaging (EPSI) volume placed using the sagittal plane of the 3D localizer image for each subject. White horizontal lines indicate the EPSI volume and cross-hatched grids show the position of the saturation band used to suppress the sinuses. Portions of the brain, largely in the frontal lobe, were also suppressed to ensure adequate suppression of sinus fluid. This results in missing experimental magnetic resonance (MR) thermometry data reflected in the comparison maps between model predicted and MR-measured temperatures (**Figure 6**). Scale bars are 50 mm.

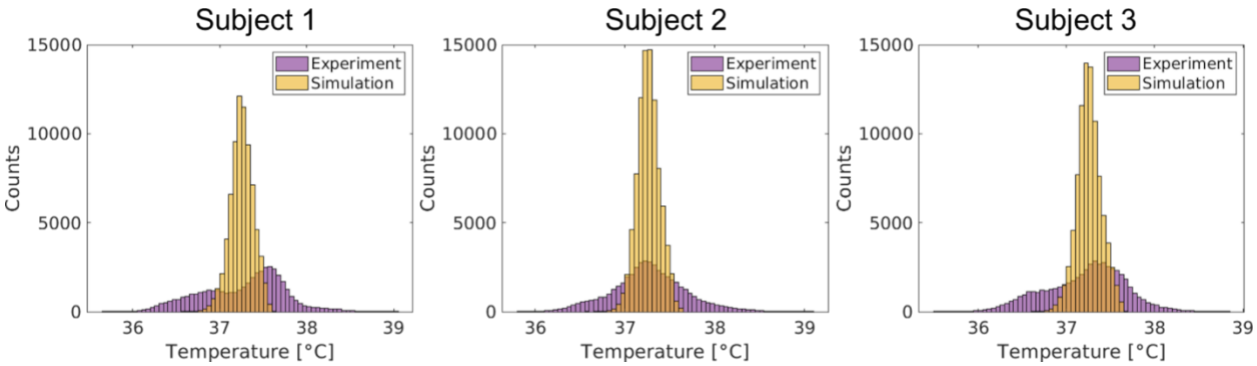

Supplementary Figure 3. Histograms of magnetic resonance (MR)-measured and model-predicted brain temperature distributions for all three subjects. Temperature distributions of MR-measured data (Experiment, purple histograms) span ~36 ˚C to 38 ˚C whereas distributions of model-predicted data (Simulation, orange histograms) fall in a narrower range of ~37 ˚C to 37.5 ˚C. Simulated temperature distributions follow a similar trend and fall within the distributions of MR-measured data. Narrower ranges of simulated distributions as compared to the experimental data are attributed to the higher apparent precision of simulations which do not reflect inherent uncertainty arising from model assumptions.

Supplementary Table 1. Vascular parameters for terminal vessel segments as a function of the number of rapidly exploring random tree (RRT) iterations.

		0	5k	10k	20k	50k	100k	200k	500k
L_{AT} (μm)	**Mean**	2199.5	2175.3	1944.8	1685.3	1349.2	1148.5	1004.4	849.8
	SD	839.1	872.7	911.2	889.7	761.5	651.6	566.2	481.6
	Med	2040.9	2578.6	2236.4	1684.8	1284.0	1091.4	953.9	803.1
	95%	3928.0	2095.6	2986.3	2966.4	2759.8	2351.3	2016.1	1721.9
	Min	1096.5	2.3	1.1	0.3	0.1	0.1	<0.1	<0.1
	Max	3978.1	3000.0	3000.0	3000.0	3000.0	3000.0	3000.0	3000.0
L_{VT} (μm)	**Mean**	4000.0	2192.1	1971.3	1694.0	1350.7	1150.7	1004.0	850.9
	SD	718.2	869.3	904.5	892.2	762.6	652.5	567.1	482.8
	Med	4109.4	2583.4	2291.3	1698.6	1282.0	1093.5	954.2	803.8
	95%	4894.3	2993.4	2987.5	2967.3	2750.6	2361.4	2020.1	1726.3
	Min	3168.1	6.6	1.7	0.5	0.1	0.1	<0.1	<0.1
	Max	4894.3	3093.4	3093.4	3093.4	3093.4	3093.4	3093.4	3093.4
D_{AT} (μm)	**Mean**	915.5	307.6	325.7	195.1	136.4	109.7	89.4	67.4
	SD	123.3	189.3	222.4	147.0	111.5	95.9	83.4	67.9
	Med	904.4	251.1	260.8	155.2	107.5	85.6	68.9	51.2
	95%	1127.5	683.3	717.6	408.5	285.8	233.2	191.5	147.8
	Min	722.2	109.2	95.7	49.1	32.7	22.2	16.8	12.0
	Max	1146.6	1822.1	2538.9	1975.2	1860.6	1880.8	1863.7	1917.9
D_{VT} (μm)	**Mean**	2109.6	595.1	459.5	341.3	314.4	198.3	168.2	137.0
	SD	91.3	501.4	405.7	317.8	309.5	200.5	181.9	161.9
	Med	2125.5	453.6	352.2	263.6	242.8	152.5	127.5	101.9
	95%	2194.9	1353.9	991.0	716.7	658.6	424.5	367.5	306.1
	Min	2007.7	135.2	101.7	84.2	65.1	30.0	28.4	20.8
	Max	2194.9	4007.6	4124.5	4081.9	5343.2	4191.8	4438.3	4737.9
CBF (mL 100 g^{-1} min^{-1})	**Mean**	118340.7	1091.9	544.3	285.7	140.5	95.6	76.2	64.9
	SD	39792.2	595.0	309.9	177.6	101.8	73.0	56.4	45.5
	Med	103993.7	949.4	470.3	239.6	108.1	73.6	62.4	59.7
	95%	188475.3	2207.3	1155.9	643.2	344.7	241.7	185.8	147.2
	Min	70496.8	8.3	2.5	0.1	0.1	<0.1	<0.1	<0.1
	Max	241934.7	9460.4	5093.3	2138.0	1155.6	759.8	524.9	402.5
Blood transport distance (μm)	**Mean**	39006.6	4317.0	3097.8	2291.8	1601.3	1242.5	975.8	717.3
	SD	18126.9	2014.2	1364.6	938.5	642.0	495.2	384.7	278.1
	Med	39368.5	4029.1	2923.6	2194.4	1531.0	1188.0	931.4	683.9
	95%	70912.6	8049.1	5557.0	3952.4	2702.4	2086.8	1624.5	1184.7
	Min	10610.3	450.4	246.6	220.4	115.4	76.8	55.8	22.1
	Max	75914.7	15981.4	12166.9	10058.1	7976.2	6286.0	5186.0	3752.9

L_{AT}: length of terminal arterial segment; L_{VT}: length of terminal venous segment; D_{AT}: diameter of terminal arterial segment; D_{VT}: diameter of terminal venous segment; Blood transport distance: mean distance between terminal arterial segments and the nearest terminal venous segment; CBF: cerebral blood flow; SD: standard deviation; Med: Median; 95%: 95th percentile value; Min: minimum value; Max: maximum value; k represents 1,000 (i.e. 5k = 5,000); Maximum vessel length was set to 3 mm during vessel generation by RRT; Minimum vessel diameter was set to 10 μm during vessel generation by RRT.

Supplementary Table 2. Vascular parameters for terminal vessels in gray matter tissue as a function of the number of rapidly exploring random tree (RRT) iterations.

		0	5k	10k	20k	50k	100k	200k	500k
L_{AT} (μm)	**Mean**	2208.2	2154.7	1916.6	1649.1	1311.9	1115.3	979.1	831.9
	SD	854.3	871.2	908.8	878.7	737.3	621.8	540.3	464.1
	Med	2005.8	2548.3	2155.0	1630.1	1252.8	1068.4	937.4	790.8
	95%	3935.2	2992.3	2984.5	2958.5	2684.0	2228.6	1937.7	1668.9
	Min	1096.5	5.3	1.1	0.3	0.1	0.1	<0.1	<0.1
	Max	3978.1	3000.0	3000.0	3000.0	3000.0	3000.0	3000.0	3000.0
L_{VT} (μm)	**Mean**	4170.9	2161.5	1939.8	1659.2	1315.4	1119.4	978.6	833.2
	SD	713.0	878.2	906.1	882.0	740.3	623.6	541.1	465.2
	Med	4316.9	2556.6	2218.7	1648.9	1251.2	1072.4	937.8	788.3
	95%	4890.7	2992.7	2986.0	2959.0	2687.2	2237.5	1939.2	1673.1
	Min	3356.0	6.6	1.8	0.5	0.2	0.1	<0.1	<0.1
	Max	4890.7	3000.0	3000.0	3000.0	3000.0	3000.0	2999.9	2999.9
D_{AT} (μm)	**Mean**	913.3	306.3	324.3	194.3	135.8	109.5	89.7	67.8
	SD	125.3	193.2	224.6	148.1	111.6	96.0	83.7	68.2
	Med	907.1	248.4	259.9	154.8	107.3	85.5	69.2	51.6
	95%	1130.7	693.6	707.3	402.7	281.6	231.5	191.6	148.9
	Min	722.2	109.2	95.7	49.1	32.7	22.2	16.8	12.0
	Max	1146.6	1822.1	2538.9	1975.2	1860.6	1880.8	1857.4	1908.6
D_{VT} (μm)	**Mean**	2113.2	593.2	455.9	337.6	312.9	197.8	168.7	137.8
	SD	101.0	517.3	411.1	318.5	309.8	201.0	182.2	162.1
	Med	2137.3	447.3	349.1	262.8	242.3	152.5	128.1	102.7
	95%	2193.9	1352.2	955.5	688.8	650.9	420.2	368.8	308.6
	Min	2023.9	135.2	101.7	87.2	69.9	30.0	28.4	20.8
	Max	2193.9	4007.6	4124.5	4081.9	5343.2	4191.8	4438.3	4737.9
CBF (mL 100 g^{-1} min^{-1})	**Mean**	117787.3	1089.5	546.8	288.5	144.7	102.1	86.9	83.5
	SD	40467.3	587.4	315.2	181.7	105.3	76.0	57.5	40.8
	Med	101035.9	947.0	469.9	240.0	111.7	80.7	75.7	79.0
	95%	190702.0	2206.2	1171.2	654.2	355.2	253.0	196.1	157.1
	Min	70496.8	8.3	2.5	0.1	0.1	<0.1	<0.1	0.3
	Max	241934.7	6884.3	5093.3	2138.0	1154.7	756.3	524.9	402.5
Blood transport distance (μm)	**Mean**	39394.8	4168.1	2995.8	2221.9	1543.8	1193.5	933.4	684.1
	SD	18391.9	1924.8	1282.8	870.4	572.7	430.8	324.4	228.6
	Med	38770.0	3884.8	2833.9	2144.9	1494.4	1159.0	908.4	667.0
	95%	71528.4	7759.5	5362.8	3786.3	2552.3	1952.8	1503.3	1084.3
	Min	10610.3	450.4	246.6	220.4	133.8	76.8	55.8	25.5
	Max	75914.7	12736.2	9065.1	6741.8	5829.9	5102.0	3274.7	2297.4

L_{AT}: length of terminal arterial segment; L_{VT}: length of terminal venous segment; D_{AT}: diameter of terminal arterial segment; D_{VT}: diameter of terminal venous segment; Blood transport distance: mean distance between terminal arterial segments and the nearest terminal venous segment; CBF: cerebral blood flow; SD: standard deviation; Med: Median; 95%: 95th percentile value; Min: minimum value; Max: maximum value; k represents 1,000 (i.e. 5k = 5,000); Maximum vessel length was set to 3 mm during vessel generation by RRT; Minimum vessel diameter was set to 10 μm during vessel generation by RRT.

Supplementary Table 3. Vascular parameters for terminal vessels in white matter tissue as a function of the number of rapidly exploring random tree (RRT) iterations.

		0	5k	10k	20k	50k	100k	200k	500k
L_{AT} (μm)	**Mean**	2047.8	2299.7	2166.3	2010.8	1740.7	1514.4	1289.9	1054.0
	SD	60.2	872.0	899.8	922.0	890.3	834.0	744.6	613.9
	Med	2047.8	2675.9	2587.9	2380.9	1769.3	1458.4	1218.2	994.7
	95%	2090.3	2995.4	2993.0	2990.1	2968.7	2909.3	2727.0	2197.5
	Min	2005.2	5.2	10.9	1.7	2.4	1.0	0.1	0.2
	Max	2090.3	3000.0	3000.0	3000.0	3000.0	3000.0	3000.0	3000.0
L_{VT} (μm)	**Mean**	3396.8	2372.2	2212.7	2007.5	1716.2	1499.8	1292.7	1054.3
	SD	689.9	793.8	854.3	922.6	884.3	839.1	746.9	616.5
	Med	2998.4	2695.0	2595.1	2359.0	1745.6	1436.4	1216.5	994.5
	95%	4193.4	2996.8	2993.5	2990.4	2964.5	2911.4	2728.4	8562.2
	Min	2998.4	39.3	15.7	3.4	0.3	0.2	0.2	0.1
	Max	4193.4	3093.4	3093.4	3093.4	3093.4	3093.4	3093.4	3093.4
D_{AT} (μm)	**Mean**	911.8	316.6	336.8	202.3	142.5	111.9	86.8	62.8
	SD	9.4	163.8	204.7	136.8	109.6	94.6	80.5	65.0
	Med	911.8	268.1	268.4	159.0	109.9	85.9	66.8	48.1
	95%	918.4	623.6	762.9	441.1	331.5	258.3	188.4	129.6
	Min	905.2	160.5	143.4	85.4	43.0	31.2	23.9	14.9
	Max	918.4	1361.3	1784.4	1672.1	1712.8	1756.2	1699.8	1700.9
D_{VT} (μm)	**Mean**	1603.6	604.8	484.2	371.3	328.6	206.5	163.1	128.5
	SD	40.2	406.9	363.2	308.1	305.9	194.1	178.8	158.6
	Med	1580.4	484.1	372.5	274.7	247.0	152.0	122.5	95.8
	95%	1650.1	1343.5	1078.3	902.6	748.2	479.3	355.9	269.1
	Min	1580.4	249.9	172.2	101.4	74.8	58.9	40.1	27.7
	Max	1650.1	3423.5	3586.3	3568.4	4680.4	3607.5	4166.3	4132.8
CBF (mL 100 g^{-1} min^{-1})	**Mean**	126552.1	1106.5	527.9	266.2	113.9	62.8	36.8	21.3
	SD	2488.0	636.6	273.3	144.9	70.4	41.4	27.0	17.2
	Med	127988.5	954.8	471.3	237.1	98.1	52.8	29.1	15.8
	95%	127988.5	2227.9	1024.5	528.5	252.2	146.9	91.6	56.5
	Min	123679.2	72.1	12.7	2.1	0.5	0.3	0.1	<0.1
	Max	127988.5	9057.3	2932.8	1583.0	1027.2	568.9	387.7	168.2
Blood transport distance (μm)	**Mean**	33228.6	5211.4	3898.0	2802.8	2206.0	1782.4	1454.6	1098.9
	SD	2058.0	2289.2	1676.5	1245.9	945.1	764.6	617.3	454.3
	Med	33228.6	4973.3	3765.6	2745.1	2054.4	1660.8	1355.7	1025.6
	95%	34674.8	9092.2	6854.6	5156.1	3930.4	3251.5	2647.3	1972.8
	Min	31773.4	803.0	559.3	389.4	199.0	167.6	123.4	61.1
	Max	34683.8	15981.4	12166.9	9791.4	7976.2	6286.0	5186.0	3752.9

L_{AT}: length of terminal arterial segment; L_{VT}: length of terminal venous segment; D_{AT}: diameter of terminal arterial segment; D_{VT}: diameter of terminal venous segment; Blood transport distance: mean distance between terminal arterial segments and the nearest terminal venous segment; CBF: cerebral blood flow; SD: standard deviation; Med: Median; 95%: 95th percentile value; Min: minimum value; Max: maximum value; k represents 1,000 (i.e. 5k = 5,000); Maximum vessel length was set to 3 mm during vessel generation by RRT; Minimum vessel diameter was set to 10 μm during vessel generation by RRT.

Supplementary Table 4. Mean axillary, core body, magnetic resonance (MR)-measured whole brain, and model-predicted whole brain temperatures, and RMSD between MR-measured and model-predicted temperatures for each subject.

	Axillary T (°C)	Core body T (°C)*	MR-measured Brain T (°C)	Model-predicted Brain T (°C)	RMSD (°C)
Subject 1	35.7 ± 0.1	36.8 ± 0.1	37.3 ± 0.5	37.3 ± 0.1	0.5
Subject 2	36.1 ± 0.3	37.2 ± 0.3	37.3 ± 0.4	37.3 ± 0.1	0.4
Subject 3	36.0 ± 0.2	37.1 ± 0.2	37.2 ± 0.5	37.3 ± 0.1	0.5

T: temperature; MR: magnetic resonance; RMSD: root mean square difference; *Core body temperature was calculated from measured axillary temperature using an offset of +1.1 ˚C (Methods); Values are reported as the mean ± standard deviation.

References

1 Blowers, S. *et al.* How does blood regulate cerebral temperatures during hypothermia? *Sci. Rep.* **8**, 1-10 (2018).